Published OnlineFirst May 21, 2014; DOI: 10.1158/1078-0432.CCR-13-2846

Cancer Therapy: Preclinical

Clinical Cancer Research

Semi-Mechanistic Pharmacokinetic/Pharmacodynamic Modeling of the Antitumor Activity of LY2835219, a New Cyclin-Dependent Kinase 4/6 Inhibitor, in Mice Bearing Human Tumor Xenografts

Sonya C. Tate[1], Shufen Cai[2], Rose T. Ajamie[2], Teresa Burke[2], Richard P. Beckmann[2], Edward M. Chan[2], Alfonso De Dios[2], Graham N. Wishart[1], Lawrence M. Gelbert[2], and Damien M. Cronier[1]

Abstract

Purpose: Selective inhibition of cyclin-dependent kinases 4 and 6 (CDK4/6) represents a promising therapeutic strategy. However, despite documented evidence of clinical activity, limited information is available on the optimal dosing strategy of CDK4/6 inhibitors. Here, we present an integrated semi-mechanistic pharmacokinetic/pharmacodynamic model to characterize the quantitative pharmacology of LY2835219, a CDK4/6 inhibitor, in xenograft tumors.

Experimental Design: LY2835219 plasma concentrations were connected to CDK4/6 inhibition and cell-cycle arrest in colo-205 human colorectal xenografts by incorporating the biomarkers, phospho-(ser780)-Rb, topoisomerase II α, and phosphohistone H3, into a precursor-dependent transit compartment model. This biomarker model was then connected to tumor growth inhibition (TGI) by: (i) relating the rate of tumor growth to mitotic cell density, and (ii) incorporating a concentration-dependent mixed cytostatic/cytotoxic effect driving quiescence and cell death at high doses. Model validation was evaluated by predicting LY2835219-mediated antitumor effect in A375 human melanoma xenografts.

Results: The model successfully described LY2835219-mediated CDK4/6 inhibition, cell-cycle arrest, and TGI in colo-205, and was validated in A375. The model also demonstrated that a chronic dosing strategy achieving minimum steady-state trough plasma concentrations of 200 ng/mL is required to maintain durable cell-cycle arrest. Quiescence and cell death can be induced by further increasing LY2835219 plasma concentrations.

Conclusions: Our model provides mechanistic insight into the quantitative pharmacology of LY2835219 and supports the therapeutic dose and chronic dosing strategy currently adopted in clinical studies. *Clin Cancer Res; 20(14); 3763–74. ©2014 AACR.*

Introduction

Since its discovery almost 30 years ago (1), the retinoblastoma protein (Rb) has received considerable attention for its role in cell-cycle control within the Rb pathway (2–4). In early G_1-phase, Rb binds to the transcription factor E2F1 and prevents the cell from transcribing the proteins required to progress into S-phase (5). Phosphorylation of Rb by cyclin-dependent kinases 4 and 6 (CDK4/6) destabilizes the Rb–E2F1 complex, thereby allowing E2F1-dependent transcription to resume (4). This enables the cell to pass through the G_1 restriction point into S-phase (6, 7). Deregulation of the Rb pathway leads to loss of cell-cycle control, one of the hallmarks of cancer (8), and subsequent tumorigenesis (2, 3, 9). Correspondingly, functional loss of the Rb pathway has been observed in a wide range of malignancies, including non–small cell lung cancer, breast cancer, and malignant glioma (2).

Given its importance in cell-cycle control (4) and the prevalence of pathway deregulation in a wide range of cancers (2), the Rb pathway is considered a highly validated anticancer drug target (10, 11). Selective inhibition of CDK4/6, the kinases responsible for phosphorylation of Rb and subsequent progression of the cell through the G_1 restriction point, represents a therapeutic strategy of great interest. Accordingly, there are a number of CDK4/6 inhibitors in development, including LY2835219, which have

Authors' Affiliations: [1]Eli Lilly and Company, Windlesham, United Kingdom; and [2]Eli Lilly and Company, Indianapolis, Indiana

Note: Supplementary data for this article are available at Clinical Cancer Research Online (http://clincancerres.aacrjournals.org/).

Current address for L.M. Gelbert: Department of Pediatrics, Indiana University School of Medicine, Indianapolis, Indiana.

Corresponding Author: Sonya C. Tate, Global PK/PD, Eli Lilly and Company, Erl Wood Manor, Windlesham, Surrey, GU20 6PH, United Kingdom. Phone: 44-1276-484503; Fax: 44-1276-483588; E-mail: tate_sonya@network.lilly.com

doi: 10.1158/1078-0432.CCR-13-2846

Published OnlineFirst May 21, 2014; DOI: 10.1158/1078-0432.CCR-13-2846

Translational Relevance

Selective inhibition of cyclin-dependent kinases 4 and 6 (CDK4/6) represents a therapeutic strategy of great interest. However, despite evidence of clinical activity, limited information is available on the quantitative pharmacology of CDK4/6 inhibitors. Here, we present an integrated pharmacokinetic/pharmacodynamic model that quantitatively relates LY2835219 plasma concentrations to CDK4/6 inhibition, cell-cycle arrest, and subsequent growth inhibition of xenograft tumors. The model indicates that chronic dosing is required to achieve durable cell-cycle inhibition associated with *in vivo* efficacy and provides insight into the plasma concentrations associated with cell-cycle arrest. It also suggests that there may be benefit in increasing plasma concentrations beyond levels yielding maximum cell-cycle inhibition. Overall, this study provides a mechanistic and quantitative characterization of LY2835219 antitumor activity, which informs and supports the dosing strategy in ongoing clinical studies.

been shown to prevent phosphorylation of Rb, induce cell-cycle arrest, and inhibit tumor growth in preclinical models (10–12). However, despite documented evidence of clinical activity (13, 14), *in vivo* characterization of the quantitative pharmacology of CDK4/6 inhibitors by means of pharmacokinetic/pharmacodynamic (PK/PD) modeling has not to our knowledge been published.

The objective of this study was therefore to characterize the PK/PD relationship of LY2835219 for CDK4/6 inhibition, cell-cycle arrest, and tumor growth inhibition (TGI) using a semi-mechanistic PK/PD model. The time-course of LY2835219 in plasma was first described by a PK model incorporating two routes of absorption to account for the unusual absorption profile exhibited by this molecule. Second, the time- and concentration-dependent effects of LY2835219 on *in vivo* target inhibition and resulting cell-cycle arrest in colo-205 xenograft tumors were described by a PD model incorporating phospho-(ser780)-Rb (p-Rb) and phenotypic biomarkers describing cell-cycle dynamics. Third, the effect of LY2835219 on the growth of colo-205 xenograft tumors was quantitatively connected to drug-dependent target inhibition and cell-cycle arrest. An additional concentration-dependent mathematical term driving quiescence and cell death was incorporated to explain further shrinkage and protracted inhibition of tumor growth observed at 100 mg/kg, which could not be accounted for by cell-cycle arrest alone. Finally, to demonstrate the predictive utility of the resulting integrated model, the cell-cycle dynamics and growth curves of A375 xenograft tumors were simulated. To our knowledge, this study not only represents the first PK/PD model describing the quantitative pharmacology of a CDK4/6 inhibitor, but also represents the first example of incorporating phenotypic biomarkers into a PK/PD model describing drug-induced cell-cycle arrest and its effect on tumor growth kinetics.

Materials and Methods

In vivo experiments

PK experiments. To assess PK in mouse, LY2835219 was administered as a single i.v. bolus dose of 1 mg/kg or as a single oral dose of 3, 12.5, 25, and 50 mg/kg ($n = 9$ for each dose). Two to three blood samples were collected from each mouse using a staggered sampling strategy at 0.25, 0.5, 1, 2, 4, 8, 12, and 24 hours after dose with an additional collection at 0.08 hours for the i.v. dose.

CDK4/6 and cell-cycle inhibition in colo-205 xenograft tumors. The extent and duration of LY2835219-mediated inhibition of CDK4/6 was assessed by quantification of p-Rb expression, which is specific for CDK4/6 and peaks in late G_1 (7), in a series of dose-response and time-course studies in mice bearing colo-205 xenograft tumors. The resultant arrest of the cell cycle was evaluated by expression of topoisomerase II α (TopoIIα) and phosphohistone H3 (pHH3) as markers of active progression through the S and G_2–M phases of the cell cycle, respectively. A standard dose range and sampling strategy was used in the initial experiments to verify target engagement; further studies made use of existing data to refine dose and time point selection. Further experimental details are provided in the Supplementary Data. A summary of the available data is provided in Supplementary Table S1.

TGI in colo-205 xenograft tumors. LY2835219 was administered daily for 21 days at 25, 50, and 100 mg/kg and compared with control tumor growth in mice bearing xenograft tumors ($n = 8$ per dose level). Doses were selected on the basis of assumed p-Rb inhibition requirements for efficacy. A further two groups of mice received 100 mg/kg of LY2835219 for either 14 or 21 days for biomarker determination ($n = 5$ per group); an additional control group was included for comparison ($n = 8$). Tumor size was measured every 2 to 7 days for 12 weeks after the first dose.

Cell-cycle and TGI in A375 xenograft tumors. Cell-cycle inhibition in A375 xenograft tumors was assessed by quantification of p-Rb, TopoIIα, and pHH3 in a dose-response study. Tumor tissue was collected at 24 hours after the last dose, following three oral doses of 22.5, 45, and 90 mg/kg of LY2835219 ($n = 5$ per dose level). Tumor growth was assessed in mice receiving vehicle, 45, or 90 mg/kg of LY2835219 daily for 21 days ($n = 8$ per dose level). Tumor size was measured every 3 to 4 days for 8 weeks after the first dose.

Development of the integrated semi-mechanistic PK/PD model

PK model. The disposition of LY2835219 was described by a two-compartment model with saturable clearance. To account for an increasingly prominent second peak at higher doses, two routes of absorption were incorporated into the model: a fast, saturable absorption route directly into the central compartment and a slow,

Published OnlineFirst May 21, 2014; DOI: 10.1158/1078-0432.CCR-13-2846

linear absorption route via five transit compartments (Fig. 1). The PK model is described by the following differential equations:

$$\frac{dA_{\mathrm{Gut}}}{dt} = -\left(\frac{V_{\mathrm{max,abs}} \cdot A_{\mathrm{Gut}}}{K_{\mathrm{m,abs}} + A_{\mathrm{Gut}}} + k_{\mathrm{a}} \cdot A_{\mathrm{Gut}}\right) \quad (1)$$

$$\frac{dA_{\mathrm{Transit,1}}}{dt} = k_{\mathrm{a}} \cdot (A_{\mathrm{Gut}} - A_{\mathrm{Transit,1}}) \quad (2)$$

$$\frac{dA_{\mathrm{Transit},i}}{dt} = k_{\mathrm{a}} \cdot (A_{\mathrm{Transit},i-1} - A_{\mathrm{Transit},i}) \quad (3)$$

$$V_{\mathrm{Cen}} \cdot \frac{dC_{\mathrm{Cen}}}{dt} = \frac{V_{\mathrm{max,abs}} \cdot A_{\mathrm{Gut}}}{K_{\mathrm{m,abs}} + A_{\mathrm{Gut}}} + k_{\mathrm{a}} \cdot A_{\mathrm{Transit,5}} + Q \cdot (C_{\mathrm{Per}} - C_{\mathrm{Cen}}) - \frac{V_{\mathrm{max},e\,\mathrm{lim}} \cdot C_{\mathrm{Cen}}}{K_{\mathrm{m},e\,\mathrm{lim}} + C_{\mathrm{Cen}}} \quad (4)$$

$$V_{\mathrm{Per}} \cdot \frac{dC_{\mathrm{Per}}}{dt} = Q \cdot (C_{\mathrm{Cen}} - C_{\mathrm{Per}}) \quad (5)$$

A_{Gut} is the amount of drug in the gut, $V_{\mathrm{max,abs}}$ and $K_{\mathrm{m,abs}}$ describe the saturable absorption, and k_{a} denotes movement of drug from the gut into the transit compartments. For transit compartment 1 to i (where $i = 2$–5), $A_{\mathrm{Transit},i}$ is the amount of drug in each transit compartment. C_{Cen} and C_{Per} denote the drug concentration and V_{Cen} and V_{Per} denote the volume of the central and peripheral compartments. Q is the intercompartmental clearance, and $V_{\mathrm{max},e\mathrm{lim}}$ and $K_{\mathrm{m},e\mathrm{lim}}$ describe the saturable elimination clearance. Initial conditions for each PK model compartment were zero, except for A_{Gut} that was equal to the dose.

Biomarker model. The biomarker model (Fig. 1) was developed using colo-205 xenograft tumor data and is composed of four transit compartments, each corresponding to early G_1, late G_1, S, and G_2–M cell-cycle phases in a sequential, open-loop manner. The biomarkers, p-Rb, TopoIIα, and pHH3, were used to represent the change in cell phase density in late G_1, S, and G_2–M phases, respectively (6, 7, 15, 16). As the formation of p-Rb occurs at the G_1 restriction point, the drug effect was implemented on the transition between early and late G_1-phase. A precursor compartment (P; ref. 17) was used to empirically represent the accumulation of cells in early G_1, upstream of the G_1 restriction point. To avoid physiologically implausible accumulation of cells in early G_1-phase, elimination was included from the precursor compartment (k_{el}). The biomarker model is described by the following differential equations:

$$\frac{dP}{dt} = k_{\mathrm{in}} - k_{\mathrm{el}} \cdot P - k_{\mathrm{R}} \cdot P \cdot (1 - E_{\mathrm{Drug}}) \quad (6)$$

$$\frac{d\text{p-Rb}}{dt} = k_{\mathrm{R}} \cdot P \cdot (1 - E_{\mathrm{Drug}}) - k_{\mathrm{G_1S}} \cdot \text{p-Rb} \quad (7)$$

$$\frac{d\mathrm{TopoII}\alpha}{dt} = k_{\mathrm{G_1S}} \cdot \text{p-Rb} - k_{\mathrm{SG_2}} \cdot \mathrm{TopoII}\alpha \quad (8)$$

$$\frac{d\mathrm{pHH3}}{dt} = k_{\mathrm{SG_2}} \cdot \mathrm{TopoII}\alpha - k_{\mathrm{MG_1}} \cdot \mathrm{pHH3} \quad (9)$$

The zero-order input into the precursor compartment, k_{in}, and the drug effect, E_{Drug}, are defined by the following equations, where I_{max} is the maximum drug effect and IC_{50}

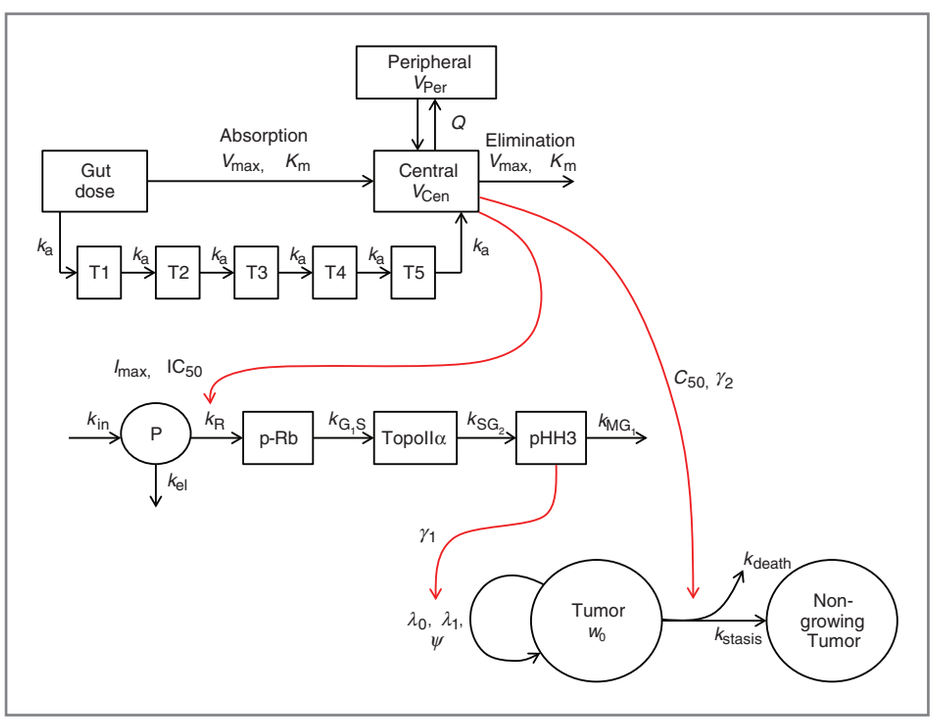

Figure 1. Schematic representation of the integrated semi-mechanistic PK/PD model for LY2835219 administered to mice bearing colo-205 xenograft tumors. Parameters are defined in the text.

Published OnlineFirst May 21, 2014; DOI: 10.1158/1078-0432.CCR-13-2846

is the drug potency:

$$k_{in} = p\text{-}Rb_0 \cdot (k_R + k_{el}) \quad (10)$$

$$E_{Drug} = \frac{I_{max} \cdot C_{Cen}}{IC_{50} + C_{Cen}} \quad (11)$$

The rate constants, k_R, k_{G_1S}, k_{SG_2}, and k_{MG_1}, drive the rate of transition of the cells through the restriction point to late G_1-phase, from late G_1 to S-phase, S-phase to G_2–M phase, and exit from G_2–M phase, respectively. The initial phase distribution of the colo-205 cell line (18) was used to adjust baseline levels of the p-Rb, TopoIIα, and pHH3 markers and to calculate the intercompartmental rate constants. Thus, the initial conditions of early G_1 (P_0), late G_1 (p-Rb_0), S (TopoIIα$_0$), and G_2–M phases (pHH3$_0$) were equal to 29.1%, 7.1%, 47.3%, and 16.5%, respectively, assuming that early G_1-phase represents 80% of total G_1-phase density. As such, the only rate constants estimated in the model are k_R and k_{el}. The remaining rate constants are calculated as follows (17):

$$k_{G_1S} = k_R \cdot \frac{P_0}{p\text{-}Rb_0} \quad (12)$$

$$k_{SG_2} = k_{G_1S} \cdot \frac{p\text{-}Rb_0}{TopoII\alpha_0} \quad (13)$$

$$k_{MG_1} = k_{SG_2} \cdot \frac{TopoII\alpha_0}{pHH3_0} \quad (14)$$

Tumor growth model. The growth rate of colo-205 xenograft tumors in control mice was described using the model previously developed by Simeoni and colleagues (19). For treated mice, it was assumed that the tumor growth inhibitory effect of LY2835219 is driven by reduced cell division as a result of cell-cycle arrest. This was incorporated mechanistically, using pHH3 as a marker for reduced density in M-phase. Two additional concentration-dependent processes were incorporated into the model to describe the extent of inhibition observed at higher doses: (i) an irreversible conversion of tumor mass from growing to nongrowing tumor cells to describe protracted TGI observed after the dosing period; and (ii) a cytotoxic component to account for the transient loss of tumor volume observed at the start of the 100 mg/kg dosing period. Growing tumor, T_g, and nongrowing tumor, T_{ng}, are described by the following differential equations:

$$\frac{dT_g}{dt} = E_{pHH3} \cdot \frac{\lambda_0 \cdot T_g}{\left[1 + \left(\frac{\lambda_0}{\lambda_1} \cdot T_g\right)^{\psi}\right]^{\frac{1}{\psi}}} - E_{[LY]} \cdot (k_{stasis} + k_{death}) \cdot T_g \quad (15)$$

$$\frac{dT_{ng}}{dt} = E_{[LY]} \cdot k_{stasis} \cdot T_g \quad (16)$$

The exponential and linear growth parameters are denoted by λ_0 and λ_1, and the cytostatic and cytotoxic effect rate constants are denoted by k_{stasis} and k_{death}. The effect of reduced mitosis on tumor growth, E_{pHH3}, is given by:

$$E_{pHH3} = \frac{pHH3^{\gamma_1}}{pHH3_0{}^{\gamma_1}} \quad (17)$$

As accelerated tumor growth was not observed upon cessation of LY2835219 treatment, the maximum allowable value of E_{pHH3} was 1. The concentration-dependent effect on tumor growth, $E_{[LY]}$, was incorporated as a nonlinear process and is defined as:

$$E_{[LY]} = \frac{C_{Cen}{}^{\gamma_2}}{C_{50}{}^{\gamma_2} + C_{Cen}{}^{\gamma_2}} \quad (18)$$

The potency and sigmoidicity of the effect of drug exposure on tumor growth are denoted by C_{50} and γ_2. The initial weight of the growing tumor (ω_0) was estimated in the model, whereas the initial weight of the nongrowing tumor was assumed to be zero. The total weight of the tumor was equal to the sum T_{ng} and T_g. A schematic of the tumor growth model is given in Fig. 1.

Model implementation and validation. The data were analyzed in a sequential manner using NONMEM VII (ICON Development Solutions). A population approach was used where longitudinal data were available. Model selection was based on goodness of fit and diagnostic plots, parameter estimate precision, the Akaike Information Criterion (AIC) value, and the Objective Function Value (OFV). Internal validation of the models was performed by graphical comparison of the raw data used to develop the model with the 5th, 50th, and 95th percentiles of 1,000 model simulations [visual predictive check (VPC)]. In addition, external validation was performed by VPC of the model versus experimental data not included in the fitting process, where available.

Results

PK model

The disposition of LY2835219 in mouse was best described by a two-compartment PK model with nonlinear clearance. The double peak absorption profile was accounted for by considering two routes of absorption: an initial saturable absorption route and a slower absorption route via transit compartments. The model successfully described the saturation of the early absorption peak and emergence of the late absorption peak at higher doses (Fig. 2). The $K_{m,abs}$ value for the fast absorption route corresponds approximately to a 9 mg/kg dose. Bioavailability was found to be, and was set equal to, 1. The model was validated internally and externally over a total dose range of 1 to 100 mg/kg of LY2835219 (Fig. 2 and Supplementary Fig. S1); the model accurately reproduced the LY2835219 plasma concentration-time profiles, with slightly inflated estimates of variability due to the sparse nature of the data.

Biomarker model

The time-course of p-Rb, TopoIIα, and pHH3 in colo-205 after oral administration of LY2835219 was best described

Published OnlineFirst May 21, 2014; DOI: 10.1158/1078-0432.CCR-13-2846

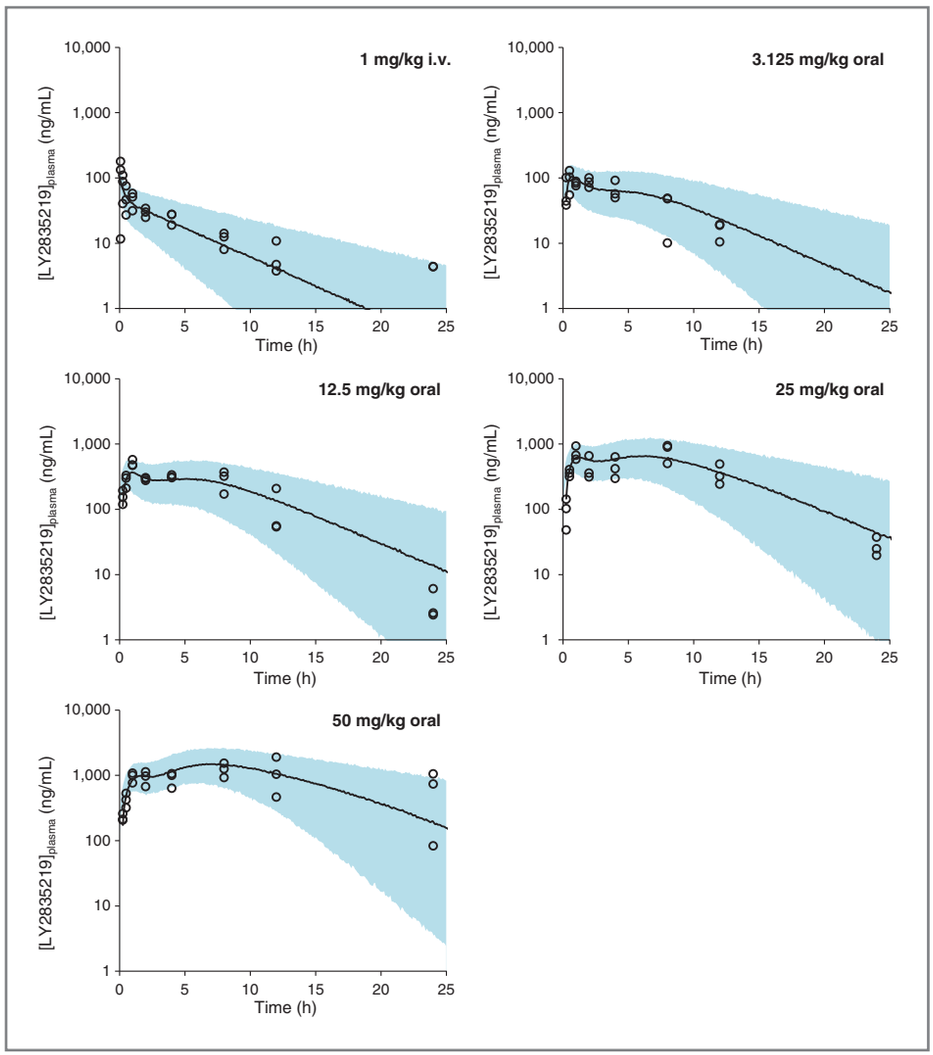

Figure 2. VPC of the PK model in normal mice following a single 1 mg/kg i.v. dose or a single 3.125, 12.5, 25, and 50 mg/kg oral dose of LY2835219. Circles, observed concentration–time data; solid line, the median of 1,000 individuals simulated by the model; and shaded area, the 5th and 95th percentiles of the 90% confidence interval around the median prediction.

by a four-compartment, precursor-dependent, indirect response model. The model successfully described the inhibition of p-Rb formation and the subsequent decrease in TopoIIα and pHH3, with maximum inhibition of each biomarker occurring at progressively later time points in accordance with the observed data (Fig. 3). The precursor compartment improved model performance by successfully accounting for the rebound observed in the biomarker levels. The I_{max} and IC_{50} estimates of 90.6% and 4.93 ng/mL are consistent with the potent and almost complete inhibition of p-Rb formation by LY2835219. The data used for the external validation were largely reproduced within the 90% confidence interval of the VPC (Supplementary Figs. S2 and S3), with some evidence of inflated variability due to the sparsity of data.

Model simulations using mean parameter estimates for colo-205 demonstrate that average p-Rb levels at steady-state decrease with dose, reaching a minimum of 30% of the control value at a dose of 50 mg/kg, corresponding to steady-state trough plasma concentrations of approximately 200 ng/mL (Supplementary Figs. S4 and S5). The amplitude of the fluctuation in p-Rb levels during the dosing interval also decreases with increasing dose, with p-Rb levels constantly maintained at their lowest value over a 24-hour period for doses above 75 mg/kg, corresponding to steady-state trough plasma concentrations above 1,000 ng/mL (Supplementary Fig. S6). The fluctuation in pHH3 levels is less pronounced, and constant maximum inhibition is achieved at doses of 50 mg/kg and above (Supplementary Fig. S6).

Tumor growth model

The time-course of control colo-205 growth was described by the model previously developed by Simeoni and colleagues (19), which provided a superior fit to a first-order growth model. The inhibitory effect of LY2835219 on tumor growth was driven by two separate components: (i) a mechanistic cytostatic component relating the rate of tumor growth to the intensity of the signal in the G_2–M phase compartment, and (ii) a nonmechanistic concentration-

Published OnlineFirst May 21, 2014; DOI: 10.1158/1078-0432.CCR-13-2846

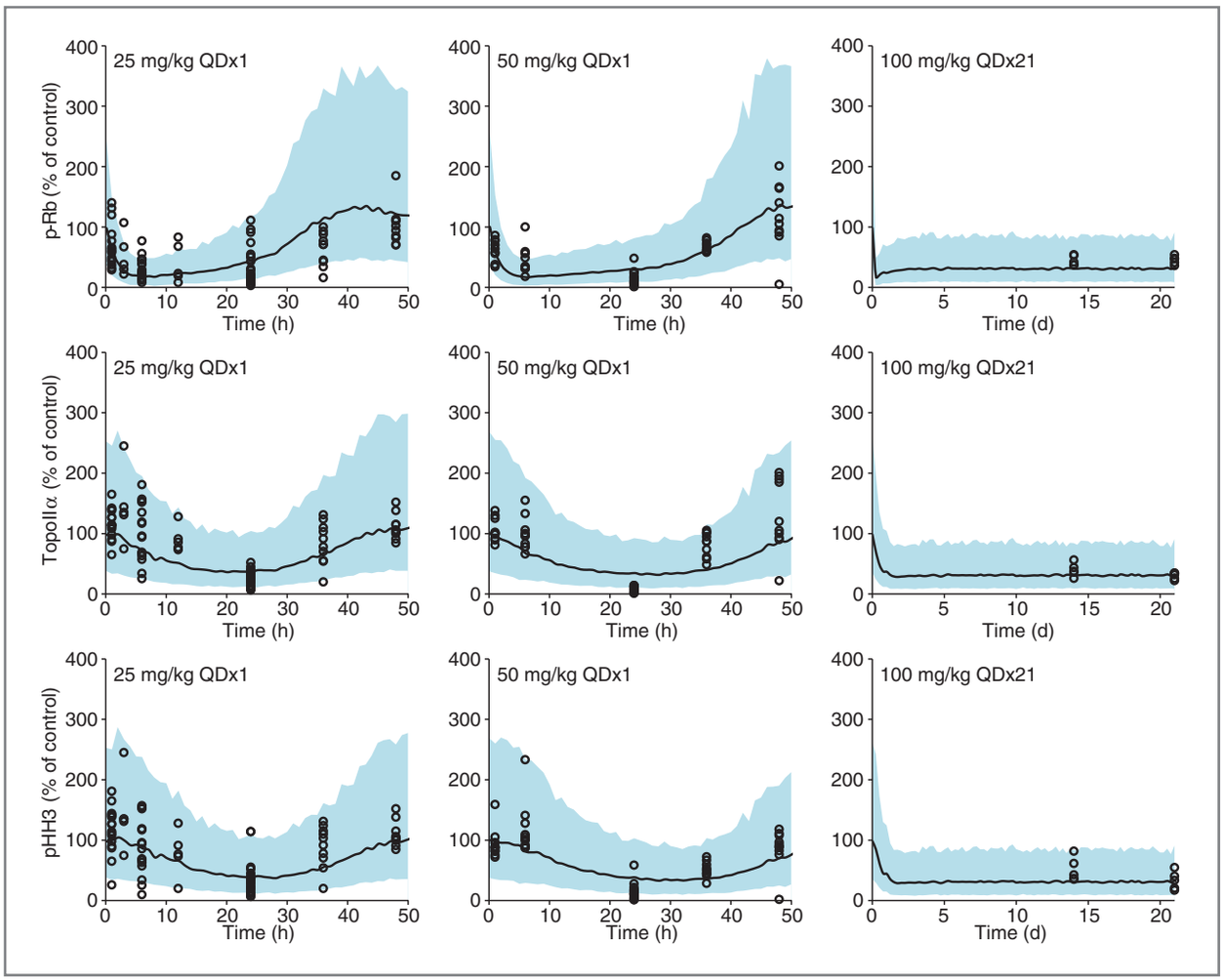

Figure 3. VPC of the biomarker model in colo-205 xenograft–bearing mice following a single 25 or 50 mg/kg oral dose of LY2835219 or a 100 mg/kg oral dose given daily for 21 days. Circles, observed p-Rb, TopoIIα, and pHH3 data in treated tumors, expressed as a percentage of the control value observed in the vehicle group; solid line, the median of 1,000 individuals simulated by the model; shaded area represents the 5th and 95th percentiles of the 90% confidence interval around the median prediction. QD, every day.

dependent mixed cytostatic and cytotoxic effect accounting for the protracted TGI observed at 100 mg/kg. This concentration-dependent process was deemed to be a sigmoidal relationship with C_{50} and γ_2 values of 1,240 ng/mL and 5, respectively, consistent with its prevalence at the highest dose. This fully integrated PK/PD model successfully described tumor size change for both control mice and for those treated chronically with LY2835219 over a 25 to 100 mg/kg oral dose range (Fig. 4).

Model simulations using mean parameter estimates for colo-205 reveal that the maximum inhibitory effect attributed to cell-cycle arrest (E_{pHH3}) is reached at a chronic dose of 50 mg/kg (Supplementary Fig. S4). TGI attributed to plasma concentration ($E_{[LY]}$) is negligible at 25 mg/kg, and although present at 50 mg/kg, $E_{[LY]}$ only reaches its full extent at 100 mg/kg (Supplementary Fig. S4). This is reflected in simulations of the tumor growth curve, where cell-cycle arrest is shown to be the primary driver of antitumor activity up to 50 mg/kg, becoming more dependent on $E_{[LY]}$ at 100 mg/kg (Supplementary Fig. S6).

Prediction of TGI in A375 xenograft tumors

The predictive utility of the integrated semi-mechanistic PK/PD model was explored by adapting it to the A375 cell line. First, the biomarker model was recalibrated by adjusting the intercompartmental rate constants based on the observed initial phase distribution of the A375 cell line. This resulted in baseline proportions of early G_1 (P_0), late G_1 (p-Rb_0), S (TopoIIα_0), and G_2–M phases (p$HH3_0$) of 59.7, 14.9, 20.7, and 4.7%, respectively (20), assuming early G_1-phase represents 80% of total G_1-phase density. The new parameter values for the rate constants, k_{G_1S}, k_{SG_2}, and k_{MG_1}, are given in Table 1. It was assumed that PK is

Published OnlineFirst May 21, 2014; DOI: 10.1158/1078-0432.CCR-13-2846

Table 1. Parameter estimates for the integrated semi-mechanistic PK/PD model for LY2835219 in mice bearing colo-205 or A375 xenograft tumors

	Colo-205 xenograft tumors		A375 xenograft tumors	
Parameter	**Estimate (SEE, %)**	**IIV, % (SEE, %)**	**Estimate (SEE, %)**	**IIV, % (SEE, %)**
PK model				
Lag time, min	8.82 (14)	—	[a]	—
$V_{max,abs}$, mg/kg/h	22.3 (24)	—	[a]	—
$K_{m,abs}$, mg/kg	9.01 (33)	—	[a]	—
k_a, h/kg	1.05 (17)	—	[a]	—
$V_{max,elim}$, μg/h/kg	4,750 (38)	34.7 (32)	[a]	
$K_{m,elim}$, ng/mL	1,160 (44)	—	[a]	—
V_{Cen}, L/kg	9.92 (19)	50.2 (34)	[a]	
Q, L/h/kg	14.3 (28)	—	[a]	—
V_{Per}, L/kg	8.56 (10)	—	[a]	—
ε_{prop}, %	19.3 (22)	—	[a]	—
Cell-cycle biomarker model				
I_{max}	0.906 (1.8)	—	[a]	—
IC_{50}, ng/mL	4.93 (21)	—	[a]	—
k_R, per hour	0.156 (6.3)	—	[a]	—
k_{G_1S}, per hour	0.639[b]	—	0.626[b]	—
k_{SG_2}, per hour	0.0960[b]	—	0.460[b]	—
k_{MG_1}, per hour	0.275[b]	—	2.04[b]	—
k_{el}, per hour	0.0482 (30)	—	[a]	—
ε_{prop}, %	61.8 (10)	—	[a]	—
ε_{add}	4.83 (8.3)	—	[a]	—
Tumor growth model				
λ_0, per day	0.0662 (4.5)	12.7 (21)	0.102 (7.6)	17.4 (32)
λ_1, mg/d	31.9 (10)	59.1 (36)	149 (9.7)	21.5 (52)
ω_o, mg	49.5 (3.4)	—	108 (7.6)	—
γ_1	0.241 (50)	—	[a]	—
C_{50}, ng/mL	1,240 (16)	—	[a]	—
k_{stasis}, per hour	0.0360 (31)	—	[a]	—
γ_2	5 (fixed)	—	[a]	—
k_{death}, per hour	0.0422 (19)	—	[a]	—
ε_{prop}, %	13.8 (7.9)	—	17.5 (14)	—

NOTE: Parameter definitions are provided in the text; further clarification is provided in Supplementary Table S2.
Abbreviations: IIV, inter-individual variability; SEE, standard error of estimate.
[a]Simulation performed using parameter estimate obtained from colo-205 xenograft tumor data.
[b]Calculated from literature baseline values of cell density in the respective cell line (18;20) using equations 12–14.
—, Not estimated or used in the model.

conserved across different xenograft tumors and that LY2835219 exerts the same extent of CDK4/6 inhibition in A375 as for colo-205. Simulations of the adapted biomarker model demonstrated prediction accuracy for both p-Rb inhibition and subsequent cell-cycle arrest over a 22.5 to 90 mg/kg dose range (Fig. 5A). The growth rate of A375 in control mice was then reestimated using the Simeoni model (Table 1; Fig. 5B; ref. 19), before connecting the adapted biomarker model described above to simulate the antitumor effect of LY2835219. This integrated model adapted to A375 cell line largely predicted LY2835219-mediated TGI at both 45 and 90 mg/kg (Fig. 5B).

Discussion

In this study, an integrated PK/PD model was developed to provide a quantitative and mechanistic description of the antitumor activity mediated by the CDK4/6 inhibitor LY2835219 in mice bearing human tumor xenografts. The resulting model is an extensive framework relating LY2835219 plasma concentrations to CDK4/6 inhibition, and to subsequent changes in cell-cycle dynamics leading to inhibited tumor growth. Although model development was based on data derived from colo-205, the semi-mechanistic nature of the model structure enabled its successful adaptation to the melanoma xenograft model A375. To our

Published OnlineFirst May 21, 2014; DOI: 10.1158/1078-0432.CCR-13-2846

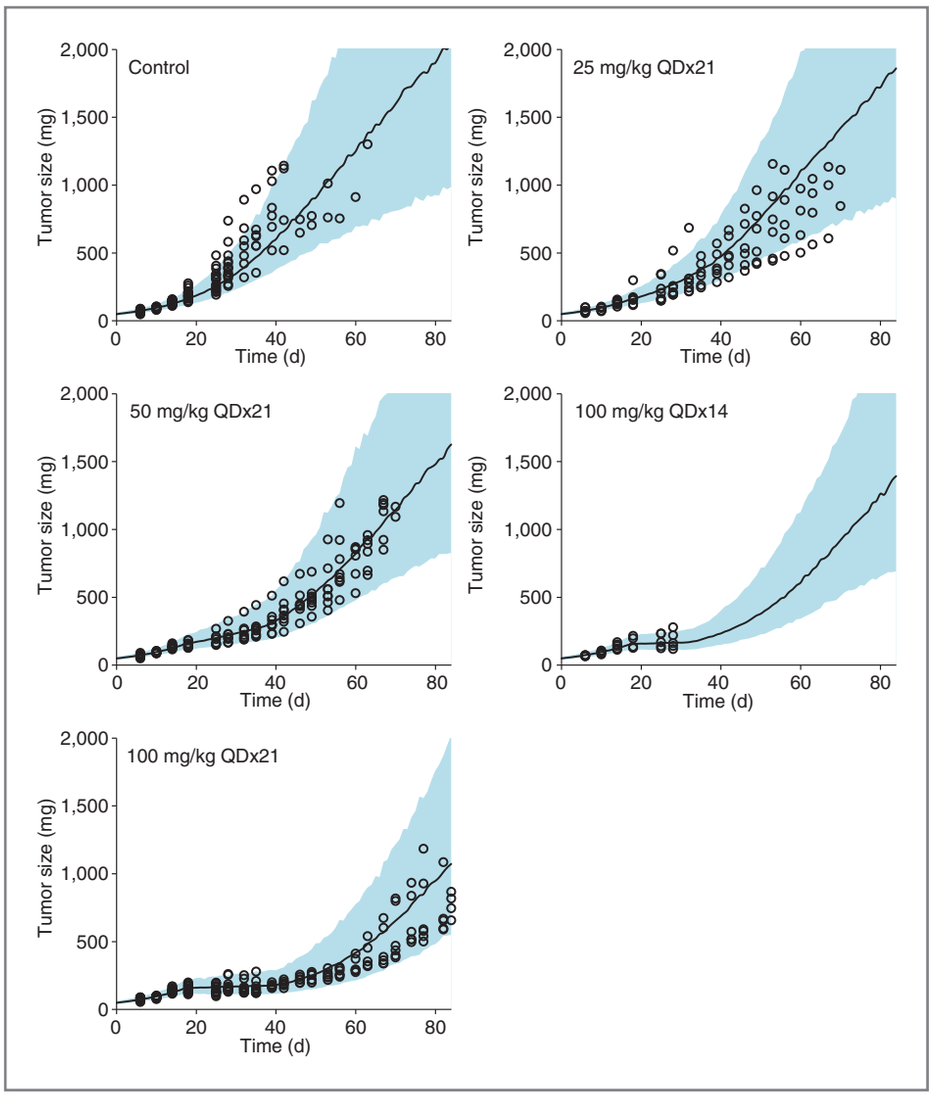

Figure 4. VPC of the tumor growth model in colo-205 xenograft-bearing mice after treatment with vehicle or with LY2835219 at 25, 50, and 100 mg/kg for 21 days, and 100 mg/kg for 14 days. Circles, observed colo-205 tumor size data; solid line, the median of 1,000 individuals simulated by the model; shaded area, the 5th and 95th percentiles of the 90% confidence interval around the median prediction. QD, every day.

knowledge, this is the first integrated approach providing a mechanistic and quantitative understanding of the PK/PD relationship of a cell-cycle inhibitor targeting the G_1 restriction point.

The semi-mechanistic PK/PD model presented in this study was developed in a sequential manner. First, a two-compartment PK model with nonlinear elimination was used to describe the disposition of LY2835219 in mouse. In addition, two routes of absorption were included in the PK model to account for the double peak phenomenon observed after oral administration. The mechanistic basis for the two peaks is currently unclear; the increasing prominence of the second peak with increasing dose suggests that enterohepatic recirculation is unlikely and potential intestinal transporters contributing to LY2835219 absorption remain unidentified. In the absence of a known mechanism, the double peak phenomenon was therefore modeled empirically, similar to a previous approach for alprazolam (21).

In the second part of this study, LY2835219 plasma concentrations were related to *in vivo* CDK4/6 inhibition in colo-205, as reflected by changes in p-Rb levels. LY2835219-mediated inhibition of p-Rb formation by CDK4/6 was best described by an indirect response model. A precursor compartment was incorporated into the model to account for the rebound in p-Rb levels observed at 48 hours after dose, which is attributed to the synchronized release into late G_1-phase of the cells arrested upstream of the restriction point. This is in agreement with previous reports of cell-cycle arrest in early G_1 induced by other CDK4/6 inhibitors (10, 22, 23). In the absence of a phenotypic biomarker for early G_1, the first-order elimination rate constant, k_{el}, was included in the precursor compartment. This resulted in a model able to reproduce the observed rebound in p-Rb, while remaining biologically plausible by preventing infinite accumulation of the cell population arrested in early G_1.

Published OnlineFirst May 21, 2014; DOI: 10.1158/1078-0432.CCR-13-2846

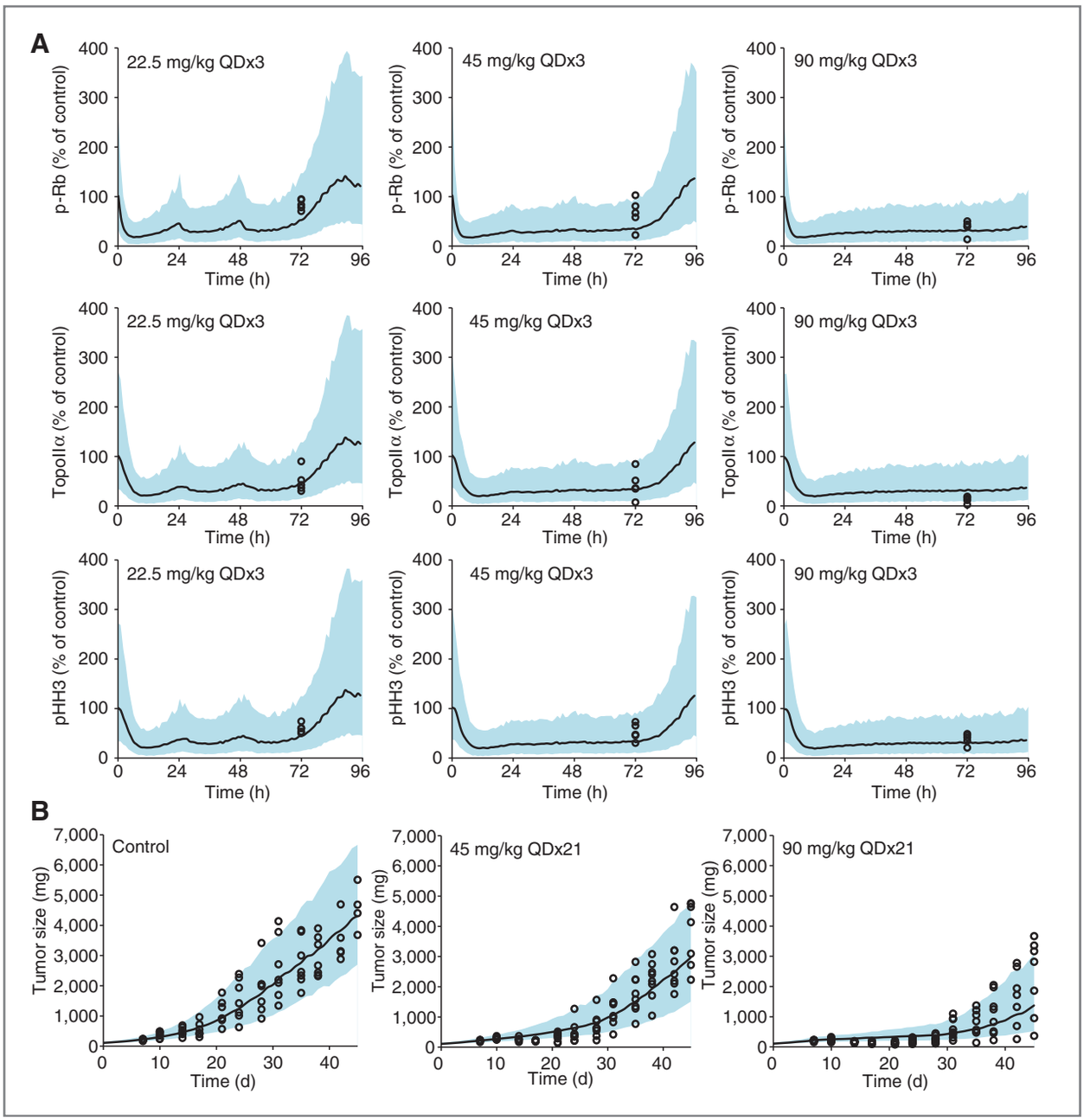

Figure 5. VPC of the integrated PK/PD model prediction of cell-cycle dynamics and TGI in A375 xenograft tumor following 22.5, 45, and 90 mg/kg of LY2835219 dosed daily for 21 days. A, circles, observed p-Rb, TopoIIα, and pHH3 data in treated A375 xenograft tumors, reported as a percentage of the control value observed in the vehicle group, following 22.5, 45, and 90 mg/kg of LY2835219 daily for 21 days. B, the circles denote observed A375 tumor size data in the groups treated with vehicle or with 45 or 90 mg/kg of LY2835219 daily for 21 days. In every panel, solid line, the median of 1,000 individuals simulated by the model; and shaded area, the 5th and 95th percentiles of the 90% confidence interval around the median prediction. QD, every day.

In addition to CDK4/6 inhibition, the model also describes the changes in cell-cycle dynamics arising from G_1 arrest by including the phenotypic biomarkers, TopoIIα (S-phase; ref. 15) and pHH3 (G_2–M phase; ref. 16), as two additional transit compartments downstream of p-Rb. As p-Rb can also be used as a phenotypic biomarker for late G_1-phase (6, 7), this extended PD model can be regarded as a simplified integrated cell-cycle model. A closed-loop system linking G_2–M phase to early G_1 phase was also tested, but proved to be too constrained to describe the downstream effects of CDK4/6 inhibition and did not improve the predictive value of the model. Mitotic doubling was not incorporated as the phenotypic biomarkers express the proportion, rather than the number of cells in each phase.

Published OnlineFirst May 21, 2014; DOI: 10.1158/1078-0432.CCR-13-2846

Despite these simplifications, the model predicted the sequential inhibition of each biomarker and the decrease in magnitude of each successive rebound after a single dose. This is in agreement with previous reports of CDK4/6 inhibition leading to sequential emptying of the cell-cycle phases downstream of the restriction point, followed by an increasing spread of cells across phases upon release from synchronization (11, 24, 25). It should be pointed out, however, that using the same rate constant between each transit compartment would not have accounted for the different duration of each cell-cycle phase (17, 26, 27). This was addressed by using the baseline phase density in the cell line (18, 20) to fix the values of the rate constants, k_{G_1S}, k_{SG_2}, and k_{MG_1}. The resulting impact on model prediction is 2-fold: (i) the model was able to account for the expected difference in transit time between the different cell-cycle compartments, and (ii) it could predict a different duration of inhibition of each phase arising from a single dose of LY2835219. In this respect, the model indicates that sustained CDK4/6 inhibition is necessary to achieve durable cell-cycle arrest, which supports the chronic dosing strategy commonly adopted for CDK4/6 inhibitors in the clinical setting (14, 28). A possible liability to fixing selected rate constants in the model is a reduced ability to capture the maximum inhibition of TopoIIα and pHH3. Nonetheless, the model remains predictive of the change in cell-cycle dynamics resulting from CDK4/6 inhibition after multiple dosing, as indicated by the external validation performed using both colo-205 and A375 data, although the extent of rebound in p-Rb immediately after chronic dosing has not been verified experimentally. Most importantly, the steady-state LY2835219 trough plasma concentrations of 200 ng/mL associated with constant cell-cycle inhibition in the model are in agreement with the clinical concentrations required for p-Rb and TopoIIα inhibition and clinical efficacy in LY2835219-treated patients (29, 30).

The third part of this study was to relate LY2835219-mediated CDK4/6 inhibition and cell-cycle arrest to TGI and predict the antitumor effect in colo-205. This was achieved by relating the rate of tumor growth to signal intensity in the G_2–M phase compartment. Further analysis of the model demonstrates, however, that while cell-cycle inhibition is the primary driver for LY2835219-mediated antitumor activity up to 50 mg/kg, it is unable to explain the protracted TGI observed at 100 mg/kg (Fig. 4 and Supplementary Fig. S6). This is in agreement with the biomarker data collected after repeated dosing of 50 and 100 mg/kg, which indicate only partial cell-cycle arrest (Fig. 3 and Supplementary Fig. S5). As a result, a nonmechanistic concentration-dependent mixed cytostatic and cytotoxic effect was incorporated into the model to account for the more profound and protracted TGI observed at 100 mg/kg. This aspect of the model suggests that increasing plasma exposure beyond that achieving maximum cell-cycle inhibition may yield additional antitumor activity in a subset of sensitive xenograft cell lines, such as colo-205 (31). Work is currently ongoing to further understand the mechanistic basis for this phenomenon; preliminary results demonstrate a sustained increase in an apoptotic biomarker, cPARP (32), and a G_0 biomarker, p130 (33), following daily dosing of 100 mg/kg in mice bearing colo-205 xenograft tumors, whereas the same increase is only transient at 50 mg/kg (data not shown). Such data support the hypothesis that sustained CDK4/6 inhibition leads to cell quiescence and cell death in sensitive xenograft tumors, such as colo-205 and A375 (31), and further support the model structure.

Finally, the integrated semi-mechanistic PK/PD model developed in this study was successfully used to predict LY2835219-mediated growth inhibition in A375 xenograft tumors. This was achieved by recalibration of the system-related parameters, including cell phase distribution and control tumor growth rate. The successful prediction of LY2835219-induced cell-cycle arrest in two cell lines suggests that our modeling framework could be used to investigate the quantitative pharmacology of CDK4/6 inhibition in other cell lines of interest. In addition, the model could potentially be broadened and adapted to other types of cell-cycle inhibitors, thereby enabling the prospective investigation of various anticancer therapeutic strategies relevant to cell-cycle inhibition. Further investigation with additional cell lines and/or cell-cycle inhibitors is warranted.

In conclusion, we have developed an integrated semi-mechanistic PK/PD model to describe and quantify the antitumor activity of LY2835219 in colo-205 and A375 xenograft tumors in mouse. The plasma concentrations of LY2835219 were related to CDK4/6 inhibition and to subsequent cell-cycle arrest, which was further connected in a quantitative manner to TGI. The resulting model represents a nested multi-scale systems pharmacology framework using middle-out principles (34). As a result, a nonclinical proof-of-concept was established and the potential of CDK4/6 inhibitors as anticancer agents was demonstrated. Moreover, this quantitative approach provides translational insight into minimally efficacious plasma exposures and supports the current clinical chronic dosing strategy as central to achieving durable cell-cycle inhibition (14, 29). Finally, the model indicates that additional antitumor activity may be achieved by escalating LY2835219 exposure beyond levels yielding an initial cytostatic effect. Overall, the modeling framework developed in this study provides a robust mechanistic and quantitative characterization of the antitumor activity mediated by the CDK4/6 inhibitor LY2835219. The model was of critical importance to inform the clinical development strategy in both a prospective and concurrent manner, namely in the use of a chronic dosing strategy, and PD biomarker selection and interpretation. It is also anticipated that this mechanistic framework may be applied to the quantitative study of cell-cycle inhibitors with alternative mechanisms to improve translation to a clinical setting.

Disclosure of Potential Conflicts of Interest

S. Cai, E.M. Chan, A. De Dios, and L.M. Gelbert are employees of Eli Lilly. R.P. Beckmann and G.N. Wishart have ownership interest (including

Published OnlineFirst May 21, 2014; DOI: 10.1158/1078-0432.CCR-13-2846

patents) in Eli Lilly Stock. No potential conflicts of interest were disclosed by the other authors.

Authors' Contributions

Conception and design: S.C. Tate, R.P. Beckmann, E.M. Chan, A. De Dios, L.M. Gelbert, D.M. Cronier

Development of methodology: S.C. Tate, T. Burke, L.M. Gelbert, D.M. Cronier

Acquisition of data (provided animals, acquired and managed patients, provided facilities, etc.): S. Cai, T. Burke, G.N. Wishart, L.M. Gelbert

Analysis and interpretation of data (e.g., statistical analysis, biostatistics, computational analysis): S.C. Tate, S. Cai, R.T. Ajamie, T. Burke, R.P. Beckmann, E.M. Chan, G.N. Wishart, L.M. Gelbert, D.M. Cronier

Writing, review, and/or revision of the manuscript: S.C. Tate, T. Burke, R.P. Beckmann, E.M. Chan, A. De Dios, G.N. Wishart, L.M. Gelbert, D.M. Cronier

Administrative, technical, or material support (i.e., reporting or organizing data, constructing databases): S. Cai

Study supervision: R.P. Beckmann, D.M. Cronier

Grant Support

This study was supported by Eli Lilly.

The costs of publication of this article were defrayed in part by the payment of page charges. This article must therefore be hereby marked *advertisement* in accordance with 18 U.S.C. Section 1734 solely to indicate this fact.

Received October 16, 2013; revised April 23, 2014; accepted May 5, 2014; published OnlineFirst May 21, 2014.

References

1. Friend SH, Bernards R, Rogelj S, Weinberg RA, Rapaport JM, Albert DM, et al. A human DNA segment with properties of the gene that predisposes to retinoblastoma and osteosarcoma. Nature 1986;323:643–6.
2. Paggi MG, Baldi A, Bonetto F, Giordano A. Retinoblastoma protein family in cell cycle and cancer: a review. J Cell Biochem 1996;62:418–30.
3. Harbour JW, Dean DC. The Rb/E2F pathway: expanding roles and emerging paradigms. Genes Dev 2000;14:2393–409.
4. Shan B, Chang CY, Jones D, Lee WH. The transcription factor E2F-1 mediates the autoregulation of RB gene expression. Mol Cell Biol 1994;14:299–309.
5. Sun A, Bagella L, Tutton S, Romano G, Giordano A. From G_0 to S phase: a view of the roles played by the retinoblastoma (Rb) family members in the Rb–E2F pathway. J Cell Biochem 2007;102:1400–4.
6. DeCaprio JA, Ludlow JW, Lynch D, Furukawa Y, Griffin J, Piwnica-Worms H, et al. The product of the retinoblastoma susceptibility gene has properties of a cell cycle regulatory element. Cell 1989;58:1085–95.
7. Kitagawa M, Higashi H, Jung HK, Suzuki-Takahashi I, Ikeda M, Tamai K, et al. The consensus motif for phosphorylation by cyclin D1-Cdk4 is different from that for phosphorylation by cyclin A/E-Cdk2. EMBO J 1996;15:7060–9.
8. Hanahan D, Weinberg RA. The hallmarks of cancer. Cell 2000;100:57–70.
9. Nevins JR. The Rb/E2F pathway and cancer. Hum Mol Genet 2001;10:699–703.
10. Fry DW, Harvey PJ, Keller PR, Elliott WL, Meade M, Trachet E, et al. Specific inhibition of cyclin-dependent kinase 4/6 by PD 0332991 and associated antitumor activity in human tumor xenografts. Mol Cancer Ther 2004;3:1427–38.
11. Gelbert LM, Cai S, Lin X, Sanchez-Martinez C, del Prado M, Lallena MJ, et al. Identification and characterization of LY2835219: a potent oral inhibitor of the cyclin-dependent kinases 4 and 6 (CDK4/6) with broad *in vivo* antitumor activity [abstract]. In: Proceedings of the AACR-NCI-EORTC International Conference: Molecular Targets and Cancer Therapeutics; 2011 Nov 12–16; San Francisco, CA. Philadelphia (PA): AACR; Mol Cancer Ther 2011;10(11 Suppl):Abstract nr B233.
12. Sanchez-Martinez C, Gelbert LM, Shannon H, De Dios A, Staton BA, Ajamie RT, et al. LY2835219, a potent oral inhibitor of the cyclin-dependent kinases 4 and 6 (CDK4/6) that crosses the blood-brain barrier and demonstrates *in vivo* activity against intracranial human brain tumor xenografts [abstract]. In: Proceedings of the AACR-NCI-EORTC International Conference: Molecular Targets and Cancer Therapeutics; 2011 Nov 12–16; San Francisco, CA. Philadelphia (PA): AACR; Mol Cancer Ther 2011;10(11 Suppl):Abstract nr B234.
13. Leonard JP, LaCasce AS, Smith MR, Noy A, Chirieac LR, Rodig SJ, et al. Selective CDK4/6 inhibition with tumor responses by PD0332991 in patients with mantle cell lymphoma. Blood 2012;119:4597–607.
14. Shapiro GI, Rosen LS, Tolcher AW, Goldman JW, Gandhi L, Papadopoulos KP, et al. A first-in-human phase 1 study of the CDK4/6 inhibitor, LY2835219, for patients with advanced cancer. J Clin Oncol 31, 2013 (suppl; abstr 2500).
15. Goswami PC, Roti Roti JL, Hunt CR. The cell cycle–coupled expression of topoisomerase II alpha during S phase is regulated by mRNA stability and is disrupted by heat shock or ionizing radiation. Mol Cell Biol 1996;16:1500–8.
16. Gurley LR, Walters RA, Tobey RA. Cell cycle–specific changes in histone phosphorylation associated with cell proliferation and chromosome condensation. J Cell Biol 1974;60:356–64.
17. Sharma A, Ebling WF, Jusko WJ. Precursor-dependent indirect pharmacodynamic response model for tolerance and rebound phenomena. J Pharm Sci 1998;87:1577–84.
18. Huang WS, Wang JP, Wang T, Fang JY, Lan P, Ma JP. ShRNA-mediated gene silencing of beta-catenin inhibits growth of human colon cancer cells. World J Gastroenterol 2007;13:6581–7.
19. Simeoni M, Magni P, Cammia C, De NG, Croci V, Pesenti E, et al. Predictive pharmacokinetic–pharmacodynamic modeling of tumor growth kinetics in xenograft models after administration of anticancer agents. Cancer Res 2004;64:1094–101.
20. Lam TL, Wong GK, Chow HY, Chong HC, Chow TL, Kwok SY, et al. Recombinant human arginase inhibits the *in vitro* and *in vivo* proliferation of human melanoma by inducing cell cycle arrest and apoptosis. Pigment Cell Melanoma Res 2011;24:366–76.
21. Wang Y, Roy A, Sun L, Lau CE. A double-peak phenomenon in the pharmacokinetics of alprazolam after oral administration. Drug Metab Dispos 1999;27:855–9.
22. Shapiro GI, Edwards CD, Ewen ME, Rollins BJ. p16INK4A participates in a G_1 arrest checkpoint in response to DNA damage. Mol Cell Biol 1998;18:378–87.
23. Fry DW, Bedford DC, Harvey PH, Fritsch A, Keller PR, Wu Z, et al. Cell cycle and biochemical effects of PD 0183812. A potent inhibitor of the cyclin D-dependent kinases CDK4 and CDK6. J Biol Chem 2001;276:16617–23.
24. Liliensiek SJ, Schell K, Howard E, Nealey P, Murphy CJ. Cell sorting but not serum starvation is effective for SV40 human corneal epithelial cell cycle synchronization. Exp Eye Res 2006;83:61–8.
25. Chen M, Huang J, Yang X, Liu B, Zhang W, Huang L, et al. Serum starvation induced cell cycle synchronization facilitates human somatic cells reprogramming. PLoS ONE 2012;7:e28203.
26. Sun YN, Jusko WJ. Transit compartments versus gamma distribution function to model signal transduction processes in pharmacodynamics. J Pharm Sci 1998;87:732–7.
27. Cronier D, Gelbert L, Wishart G, De Dios A. A fully integrated PK/IVTI/IVE model in mouse to help design the FHD trial for a cell cycle inhibitor X [abstract]. In: Proceedings of the Annual Meeting of the Population Approach Group in Europe; 2009; St. Petersburg, Russia. p. 18. Abstract nr 1611.
28. Flaherty KT, Lorusso PM, Demichele A, Abramson VG, Courtney R, Randolph SS, et al. Phase I, dose-escalation trial of the oral cyclin-dependent kinase 4/6 inhibitor PD 0332991, administered using a 21-day schedule in patients with advanced cancer. Clin Cancer Res 2012;18:568–76.
29. Patnaik A, Rosen LS, Tolaney SM, Tolcher AW, Goldman JW, Gandhi L, et al. Clinical activity of LY2835219, a novel cell cycle inhibitor

Published OnlineFirst May 21, 2014; DOI: 10.1158/1078-0432.CCR-13-2846

selective for CDK4 and CDK6, in patients with metastatic breast cancer [abstract]. In: Proceedings of the Annual Meeting of the American Association for Cancer Research; 2014 Apr 5–9; San Diego, CA. Philadelphia (PA): AACR; 2014. Abstract nr CT232.

30. Rosen LS, Shapiro GI, Tolcher AW, Goldman JW, Gandhi L, Papadopoulos KP , et al. Early development of LY2835219, a novel cell cycle inhibitor with activity against CDK4 and CDK6 [abstract]. 12th International congress on Targeted Anticancer Therapies 2014 Mar 5. Abstract nr O4.3.
31. Dempsey JA, Chan EM, Burke TF, Beckmann RP. LY2835219, a selective inhibitor of CDK4 and CDK6, inhibits growth in preclinical models of human cancer [abstract]. In: Proceedings of the 104th Annual Meeting of the American Association for Cancer Research; 2013 Apr 6-10; Washington, DC. Philadelphia (PA): AACR; Cancer Res 2013;73(8 Suppl):Abstract nr LB-122.
32. Kaufmann SH, Desnoyers S, Ottaviano Y, Davidson NE, Poirier GG. Specific proteolytic cleavage of poly(ADP-ribose) polymerase: an early marker of chemotherapy-induced apoptosis. Cancer Res 1993;53:3976–85.
33. Smith EJ, Leone G, DeGregori J, Jakoi L, Nevins JR. The accumulation of an E2F-p130 transcriptional repressor distinguishes a G_0 cell state from a G_1 cell state. Mol Cell Biol 1996;16:6965–76.
34. Noble D. Systems biology and the heart. Biosystems 2006;83:75–80.

Published OnlineFirst May 21, 2014; DOI: 10.1158/1078-0432.CCR-13-2846

Clinical Cancer Research

Semi-Mechanistic Pharmacokinetic/Pharmacodynamic Modeling of the Antitumor Activity of LY2835219, a New Cyclin-Dependent Kinase 4/6 Inhibitor, in Mice Bearing Human Tumor Xenografts

Sonya C. Tate, Shufen Cai, Rose T. Ajamie, et al.

Clin Cancer Res 2014;20:3763-3774. Published OnlineFirst May 21, 2014.